Proceedings of the 50th International School & Conference on the Physics of Semiconductors

Structure, Optical and Photocatalytic Properties of ZnO Nanostructures Grown on Ag-Coated Si Substrates

V. Karpyna[a], L. Myroniuk[a,*], O. Bykov[a], D. Myroniuk[a], O. Kolomys[b], V. Strelchuk[b], L. Petrosian[a] and A. Ievtushenko[a]

[a] *I. M. Frantsevich Institute for Problems in Materials Science, NAS of Ukraine, 3 Krzhyzhanovsky str., 03142 Kyiv, Ukraine*
[b] *V.E. Lashkaryov Institute of Semiconductor Physics, NAS of Ukraine, 41 Nauky av., 03028, Kyiv, Ukraine*

Doi: 10.12693/APhysPolA.142.644 *e-mail: liliiamolotovska@gmail.com

The effect of annealing on the optical properties of zinc oxide nanostructures grown by atmospheric pressure metalorganic chemical vapor deposition on silicon substrates covered with a thin film of silver is investigated. It is shown that annealing at temperatures above 600°C significantly reduces the concentration of oxygen vacancies, and as a result, the ratio of the integrated intensity of ultraviolet emission to visible is improved 4.3 times. As a result of further high-temperature annealing at 900°C, the excitonic emission peak at 378 nm in the photoluminescence spectra is observed to shift towards larger wavelengths to 380 nm. Simultaneously, a decrease in its half-width from 140 to 100 nm is observed, which indicates an improvement in the structural perfection of ZnO/Ag/Si nanostructures. At the same time, an additional band in the region of 475 nm appeared, which, as we suggest, is due to optical transitions from the levels of shallow donors to the acceptor level created by the diffusion of silver in the lattice of zinc oxide. Annealing of ZnO nanostructures grown on silicon substrates as well as Ag-coated Si substrates improves their structure and optical properties, but unfortunately, this leads to a reduction in the photocatalytic activity of prepared ZnO nanostructures.

topics: ZnO, nanostructures, photoluminescence, Raman scattering

1. Introduction

Silver-doped ZnO nanostructures (NS) attract great attention in developing optoelectronic and photovoltaic devices. Because of its low toxicity and biocompatibility, ZnO is a significant material for biomedicine applications. A unique combination of optical and semiconducting properties results in high catalytic and photochemical activity in the ultraviolet (UV) region of the optical spectrum and makes silver-doped ZnO a promising photocatalytic material, essential for biological applications. Surface modification of ZnO nanostructures with Ag metal nanoparticles can significantly improve the photocatalytic efficiency due to the possible generation of localized surface plasmons, enhancing light absorption, and having a significant impact on semiconductor photocatalysis. Good photocatalytic efficiency in the process of organic dye degradation applying ZnO NS of various morphology, doped by silver nanoparticles, was shown in some papers [1–3].

Distinct ZnO NS can be obtained by various methods, including hydrothermal, spray pyrolysis, electrospinning, sol–gel, and chemical vapor deposition (CVD). In our recent paper [4], we successfully applied the metalorganic CVD method for growing silver-doped ZnO nanostructures from a mixture of zinc acetylacetonate and silver acetylacetonate precursors. It is worth noting that silver acetylacetonate precursor is very expensive. So, in this paper, we consider the growth of ZnO nanostructures from single acetylacetonate precursor on Ag-coated Si substrates and study the influence of applied annealing treatment on silver diffusion and optical and photocatalytic properties of grown ZnO NSs. Moreover, in published work [4], we supposed that Ag ions incorporate into ZnO as donor-type defects occupying interstitial sites in ZnO lattice at moderate substrate temperature, especially in the case of 1 % wt. Ag because both work function and resistivity were decreased. We believe that high-temperature annealing favors the

TABLE I

Peak position 2θ and FWHM of main XRD reflections for as-grown and annealed ZnO/Si and ZnO/Ag/Si NSs

Sample	2Θ/FWHM of main reflections[°]					
	100	002	101	100	002	101
	ZnO/Si NS			ZnO/Ag/Si NS		
As-grown	31.77/0.26	34.45/0.22	36.24/0.23	31.81/0.36	34.45/0.23	36.26/0.31
Annealed at 600°C	31.79/0.17	34.44/0.11	36.25/0.19	31.8/0.15	34.43/0.16	36.28/0.2
Annealed at 900°C	31.7/0.18	34.39/0.14	36.22/0.22	31.73/0.16	34.39/0.16	36.21/0.21

diffusion of Ag into ZnO lattice with substitution Zn sites, thus favoring the formation of an acceptor-type energy level.

2. Experimental details

ZnO nanostructures were grown on Si substrates by atmospheric pressure metalorganic chemical vapor deposition method (APMOCVD) using zinc acetylacetonate powder as a source precursor. The growth process takes place in a small quartz tube with a diameter of 26 mm, and a length of 30 cm, which was placed in the tubular furnace. On one side of this tube, the substrates were placed, and on the other side, the boat with a zinc acetylacetonate precursor powder was arranged when the temperature in the furnace reached the set temperature level (T_{set} = 400°C). Due to the existing temperature gradient along the furnace, the substrate temperature was 500°C when the temperature of the precursor boat was 300°C. The zinc acetylacetonate has a low sublimation temperature of 138°C, so the active process of evaporation and decomposition of the metalorganic compound occurs. The vapor is transported along the furnace when the released zinc metal is oxidized. The result of this process is condensing ZnO in the form of various nanostructures depending on temperature, vapor pressure, as well the nature of the substrate.

For our experiments, we used one gram of zinc acetylacetonate powder. ZnO nanostructures were grown on bare Si substrate as well as on Si substrate covered by Ag film. The film of Ag was formed by a silver mirror reaction using Tollens' reagent and glucose. To prepare this reaction, we used solutions of NaOH (10 %) and $AgNO_3$ (10 %) as well as concentrated NH_4OH and glucose solution (400 mg/ml).

In order to investigate the influence of silver diffusion on the optical properties, the obtained ZnO nanostructures were sequentially annealed in the air at two temperatures, 600 and 900°C, for 3 h.

X-ray diffraction (XRD) study was carried out on a DRON-3 diffractometer in Bragg-Brentano configuration using Cu K_α radiation ($\lambda = 0.1542$ nm). The photoluminescence (PL) of deposited films was excited using a He–Cd laser with the photon energy $h\nu$ = 3.81 eV (325 nm) at room temperature. The Raman measurements were carried out

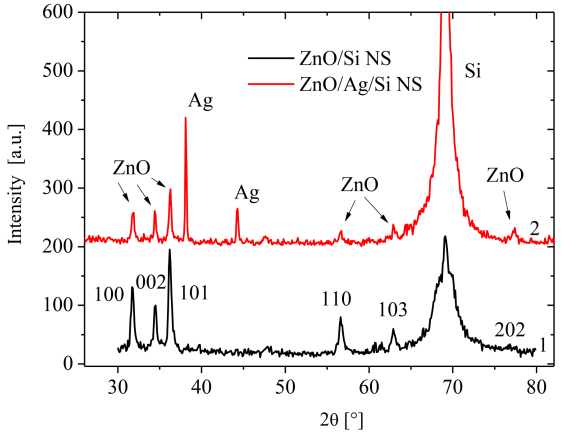

Fig. 1. XRD pattern of ZnO NS grown on Si (1) and Ag/Si (2) substrates.

in a quasi-backscattering geometry at room temperature using a Horiba Jobin Yvon T64000 triple spectrometer with integrated micro-Raman setup — Olympus BX41 microscope equipped with a motorized XYZ stage (minimum step 100 nm) and a Peltier-cooled CCD detector. The experiments were carried out using the 488 nm line of an Ar/Kr laser.

Photocatalytic activity of deposited ZnO NS was investigated by decomposition of methyl orange (MO) dye at Hg lamp irradiation (200 W) for 9 h. Every three hours, the residual concentration of dye was calculated from transmission spectra at the point of maxima dye absorption on wavelength 465 nm.

3. Results and discussion

Figure 1 shows XRD patterns of as-grown ZnO NS grown on Si and Ag/Si substrates. In both cases, the formation of zinc oxide crystallites with the structure of wurtzite can be seen. The observed X-ray reflections (100), (002), (101), and (110) belong to the hexagonal zinc oxide syngony in accordance with Powder Diffraction File (PDF) card no. 36-1451. For ZnO NS grown on Ag/Si substrate, the reflections (110) and (103) are smaller; at the same time, the intensity of (101) and (202) reflections was stronger compared to NS grown on Si. The

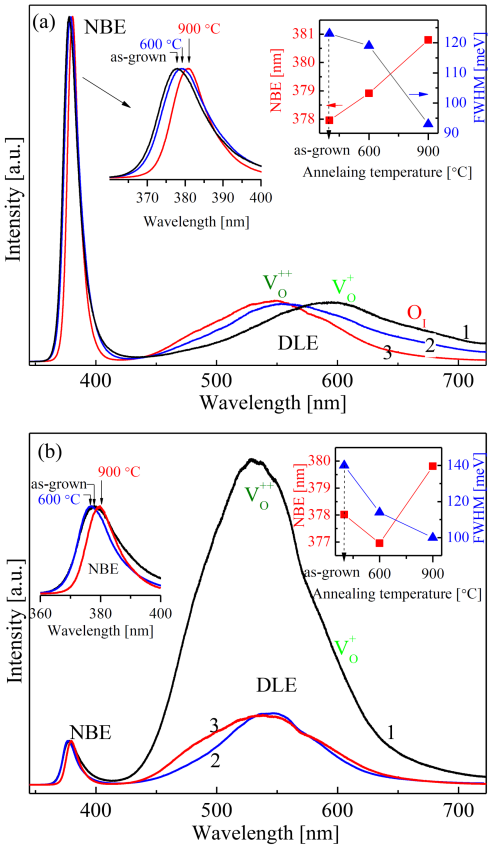

Fig. 2. Normalized room temperature PL spectra of as-grown (curve 1) and annealed (curves 2, 3) ZnO/Si NS (a) and ZnO/Ag/Si NS (b). The insets show a magnification of the NBE band region for normalized spectra and influence of annealing temperature on peak position and FWHM of NBE emission.

diffraction pattern clearly shows the reflections of X-rays from the planes of the crystal lattice of silver according to PDF card no. 04-0783, which confirms the formation of a polycrystalline film of metallic silver on a silicon substrate. Presented XRD patterns are typical for the NS grown by APMOCVD on Si, sapphire, and quartz substrates at mentioned conditions. In Table I, we have summarized the XRD data obtained for as-grown and annealed for both NS ZnO/Si and ZnO/Ag/Si. All main reflections (100), (002), and (101) demonstrate the shift to lower angles with diminishing of full width at half maximum (FWHM) parameter. This indicates the enlargement in interplane distance and volume of the primitive cell, especially for higher annealing temperatures. A significant distinction between NS grown on Si and Ag/Si substrate is not observed. Thus, we can state that the given condition of annealing does not favor the incorporation of silver ions into the crystal lattice of ZnO in the great amount due to the bigger difference between ion radii of Ag^{+} (97 pm) and Zn^{2+} (74 pm), but some diffusion between grains can be provided.

TABLE II

Integral intensity in ultraviolet I_{uv} and visible regions of PL spectra I_{vis} for ZnO/Si and ZnO/Ag/Si samples before and after annealing.

State	I_{uv} [arb. u.]	I_{vis} [arb. u.]	I_{vis}/I_{uv}
ZnO/Si			
As-grown	163	268	1.64
Annealed at 600°C	160	254	1.58
Annealed at 900°C	127	224	1.76
ZnO/Ag/Si			
As-grown	182	8721	47.92
Annealed at 600°C	157	1714	10.91
Annealed at 900°C	135	1959	14.51

Figure 2 presents PL spectra of as-grown, annealed at different temperatures ZnO/Si (a) and ZnO/Ag/Si (b) NS. In order to correctly estimate the effect of annealing, all obtained PL spectra before and after annealing were normalized to the intensity of the near-band edge (NBE) emission. As can be seen in Fig. 2, the obtained PL spectra consist of two energetically separated bands, which are observed in all the samples. The first PL band is located in the ultraviolet part of the spectrum at 377–384 nm. The other PL band is situated in the visible region of the spectrum, around 530–550 nm. The ultraviolet NBE emission is due to the radiative recombination of free excitons [5]. The broad deep-level emission (DLE) band in the visible region of the spectrum typically corresponds to the radiative recombination of intrinsic point defect, namely oxygen vacancy (V_O) in various charge states, oxygen interstitials (O_I), oxygen antisite (Zn_O), zinc vacancy (V_{Zn}), zinc interstitials (Zn_I), and zinc antisite (O_{Zn}) [6]. In the case of NSs grown under oxygen-rich conditions, it is possible to form defects O_I and V_{Zn} [7].

The main difference in the PL spectrum of as-grown ZnO/Si NS and as-grown ZnO/Ag/Si NS is the various contribution of NBE and DLE emission. In the spectrum of ZnO/Si NSs (Fig. 2a), there is an intense NBE peak at 378 nm with low intensity of the DLE band, while the PL spectrum of ZnO/Ag/Si nanostructures (Fig. 2b) shows an intense DLE band at 530 nm with low intensity of NBE emission at 378 nm. Such difference in PL spectra could be explained by a different number of intrinsic defects, which obviously depends on the nature of the substrate. The quantitative characteristic of PL is the integral intensity of PL. Table II summarizes the parameters of the integral PL intensity (I_{uv} - the integrated intensity of the ultraviolet PL, I_{vis} — the integrated PL intensity in the visible part of the spectrum) for the as-grown ZnO and annealed ZnO NS.

From the data given in Table II, it is seen that the annealing of ZnO/Si NS at a temperature of 600°C almost does not change the PL quantitative parameters. The ratio of the integrated intensity of the visible PL band to the UV band (I_{vis}/I_{uv}) is about 1.6 for both cases before and after annealing. Slightly higher values of the integrated intensity of the visible PL band are due to its wider integration range of 400–700 nm, while the integration for the UV band was carried out in a range of 360–400 nm. Lower values of I_{uv} after re-annealing of ZnO/Si NS at the temperature of 900°C are due to a decrease in the half-width of the peak, which corresponds to a decrease in the density of those states that are responsible for the boundary PL. We are talking here about those surface states that cause the expansion of the UV PL peak in the region of 390–400 nm. For ZnO/Ag/Si samples, annealing, even at a relatively low temperature of 600°C, significantly reduces the intensity of the visible deep-level PL by 5 times. It is known that PL in the region of 520–540 nm is due to oxygen vacancies. Annealing at 600°C reduces the number of oxygen vacancies and, accordingly, significantly improves the UV to visible PL ratio, namely, the I_{vis}/I_{uv} ratio is reduced from almost 48 to 11, i.e., more than 4 times. The PL spectrum of ZnO/Ag/Si NS annealed at 900°C demonstrates the appearance of a new emission band at 475 nm, which may be a result of the incorporation of silver into the zinc oxide lattice and the creation of a deep acceptor level. In this case, the optical transitions between shallow Zn_I donor levels and deep Ag_{Zn} acceptor levels are possible [8]. Therefore, the ratio of integral intensity I_{vis}/I_{uv}, due to the appearance of this new emission band, slightly increases from 10.91 to 14.51 (see Table II).

The insets in Fig. 2 show the peak position of NBE emission and FWHM parameters for ZnO/Si (Fig. 2a) and ZnO/Ag/Si (Fig. 2b) NS as a function of the annealing temperature. It can be seen in Fig. 2a that after high-temperature annealing at 900°C, there is a shift of the NBE peak of ZnO/Si NS towards greater wavelengths, from 378 to 381 nm. This change in the position of the NBE band can be attributed to the reduction of the structural defects in films, to strain relaxation, and also to the increase of grain size with annealing, which agrees with XRD results. A narrowing of the exciton band is also observed. The FWHM of the NBE emission of ZnO/Si NS decreased monotonically from 120 to 90 meV as the annealing temperature was increased, indicating that the quality of the ZnO/Si NS films improved due to a reduction in defect density. This effect was also observed for ZnO/Ag/Si NS (Fig. 2b, inset).

Finally, the method of Raman scattering was used to study the effect of thermal annealing on the crystal quality and vibrational properties of ZnO NS grown on Si and Ag/Si substrates. The studies were performed in the backscattering geometry with the z direction oriented parallel to the *c* axis of the ZnO films at room temperature. In this configuration, only E_2^{low}, E_2^{high} and A_1^{LO} modes are allowed for the ZnO wurtzite structure according to the symmetry selection rules [9]. Figure 3 shows the Raman spectra of as-grown and sequentially annealed (at temperatures of 600 and 900°C for 3 h) ZnO/Si NS and ZnO/Ag/Si NS. In the Raman spectra of ZnO NS grown on Si and Ag/Si substrates, the intensive E_2^{low} phonon mode at 98 cm^{-1}, E_2^{high} phonon mode at 437 cm^{-1}, and optical phonon mode with longitudinal oscillations $qA(E)_1^{LO}$ are observed. The E_2^{high} mode is associated exclusively with oxygen sublattice oscillations, and the E_2^{low} phonon mode is caused by oscillations in the zinc sublattice [10]. The band at 584 cm^{-1} is attributed to $qA(E)_1^{LO}$ phonon mode, and its position reflects the superposition of processes, A_1^{LO} at 574 cm^{-1} and E_1^{LO} at 586 cm^{-1}, due to the inclination of the *c* axis of ZnO crystallites from normal. The wide weak A_1^{LO} mode at 580 cm^{-1} is caused by the disorder of the crystal structure, in particular the presence of such point defects as oxygen vacancies, zinc interstitials, or their complexes, as well as the inclination of crystallites in NSs. Other bands, located at 207 and 334 cm^{-1}, were also observed in the Raman spectra of the samples. These peaks are believed to be second-order Raman scattering that arose from zone-boundary (M point) phonons $2TA(M)$ and $E_2^{\text{high}} - E_2^{\text{low}}(M)$, respectively. The bands at 380 cm^{-1} and 412 cm^{-1} are assigned to the transverse-optical mode with A_1^{TO} and the first-order transverse-optical mode with E_1^{TO}, respectively. The presence of the latter is caused by the large angular aperture of the confocal microscope objective and crystal imperfections. We used the Lorentz function to fit peak positions of phonon modes and analyze observed changes in the phonon spectrum.

The insets in Fig. 3 show the frequency positions and values of the FWHM of the E_2^{high} phonon mode in the dependence on the annealing temperature. As the annealing temperature increases, there is a low-frequency shift of the phonon mode position E_2^{high} to the frequency 436.4 cm^{-1}, which is characteristic of a ZnO single crystal, and a decrease in FWHM value, which obviously indicates relaxation of elastic deformations in the zinc oxide lattice and improvement of their crystalline perfection (reduction of the concentration of point defects).

However, as can be seen from the spectra 1 and 2 (Fig. 3b), growing ZnO NS on Ag/Si substrate leads to a significant change in the shape and intensity of E_2^{low}, E_2^{high}, and A_1^{LO} phonon modes of ZnO NS, compared to those grown on bare Si substrates (Fig. 3a). Analysis of these changes allows us to conclude that the presence of a silver film on a silicon substrate leads to an increase in disordering in the crystal structure of ZnO/Ag/Si NS compared to ZnO/Si NS. The frequency position of the weak E_2^{high} phonon mode shifts

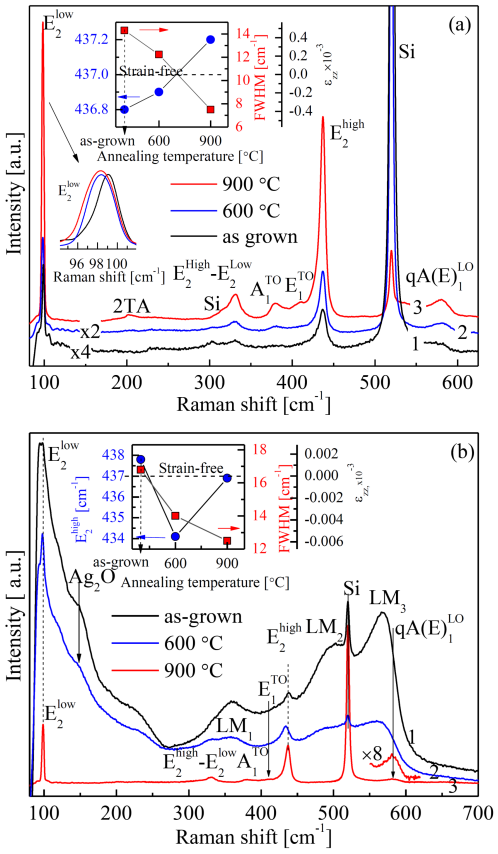

Fig. 3. Room temperature Raman spectra of as-grown (curve 1) and annealed (curve 2, 3) ZnO/Si NS (a) and ZnO/Ag/Si NS (b). In the inset, frequency position and FWHM of the E_2^{high} mode depending on the annealing temperature is shown. The inset scale shows the strain developed in NS. Tag "Si" denotes Raman bands from substrate.

toward higher frequencies (up to 438.9 cm^{-1}), and its FWHM value was increased to 15.4 cm^{-1} (see inset in Fig. 3b), compared to NS deposited on uncoated Si substrates (see inset in Fig. 3a), for which FWHM value was 9.7 cm^{-1}. The shift of E_2^{high} mode corresponds to the presence of biaxial tensile stress in the plane of the substrate. To quantitatively characterize the influences of stress on optical phonons, the frequency shift of the E_2^{high} mode, $\Delta\omega$, was analyzed as a function of lateral strain, ε_{xx} [11], as follows,

$$\Delta\omega = 2\left(a - b\frac{C_{13}}{C_{33}}\right)\varepsilon_{xx} = m\varepsilon_{xx}, \qquad (1)$$

where $\Delta\omega = \omega - \omega_0$, $\omega_0 = 437.0$ cm^{-1} $is E_2^{\text{high}}$ phonon frequency of unstrained ZnO bulk crystal, $a = -690.8$ cm^{-1} and $b = -940$ cm^{-1} — phonon deformation-potential parameters, $C_{13} = 105.1$ GPa and $C_{33} = 210.9$ GPa — elastic constants of ZnO single crystal [12], and $m = -443$ cm^{-1} — the phenomenological coefficient. Thereby, ZnO NS grown on Si substrate demonstrate the most pronounced frequency shift of E_2^{high} from 436.8 to 437.2 cm^{-1}, which corresponds to the change of ε_{xx} deformations in the range -0.4–0.4×10^{-3}. For ZnO NS deposited on Ag/Si substrate, the peak positions of E_2^{high} mode are non-monotonically shifted from 436.8 to 436.9 cm^{-1} with an abrupt decrease at 434 cm^{-1} indicated on the practical complete relaxation of elastic deformations. The anomalous decrease in the frequency of E_2^{high} mode to 434.1 cm^{-1} at an annealing temperature of 600°C can be due to the incorporation of Ag ions into the ZnO matrix. A large difference in the ionic radius of Ag^{2+} (97 pm) and Zn^{2+} (74 pm) ions leads to significant tensile strain, which is reflected in the position of the E_2^{high} band. Further increase in the annealing temperature leads to the self-cleaning of ZnO nanocrystallites due to the aggregation of silver atoms into clusters, that confirmed by XRD [13]. An increase in the annealing temperature up to 900°C causes a significant change in the shape of the Raman spectrum of ZnO NS grown on Ag/Si substrates, namely, a wide intense band in the spectral region 90–260 cm^{-1} is transformed into a narrow intense E_2^{low} mode, the phonon mode E_2^{high} increases, and A_1^{LO} mode practically disappears, which indicates a significant improvement in the crystal structure of ZnO.

Additionally, in the Raman spectra of as-grown and annealed at 600°C ZnO NS deposited on Ag/Si substrates, structured wide intense bands appear in the spectral region of 90–260 cm^{-1}. The intensive wide bands at 95 and 146 cm^{-1} are attributed to Ag lattice vibrational modes [14, 15]. Moreover, in the Raman spectra of the as-grown and annealed at 600°C ZnO/Ag/Si NS, one can see additional features at 360, 498, and 567 cm^{-1} (indicated in Fig. 3b as LM_1–LM_3). A band centered approximately at 495–500 cm^{-1} can be ascribed to surface optical phonons (SOP) formed from phonons of the symmetry A_1 or the symmetry E_1 [16]. This phonon mode cannot be a local vibrational mode associated with Ag ions, as it was also observed for ZnO doped with Mn [17] and Co [18]. SOP modes appear in polar crystals whose particle size is smaller than the wavelength of an incident laser beam. Nano-sized particles and the presence of imperfections and/or impurities result in a breakdown of phonon momentum selection rules, thus making some forbidden vibration modes contribute to Raman scattering. The high percentage of defects located in surface and grain boundaries would induce significant SOP vibration and greatly depress the vibration of the volume phonon of ZnO in the Raman scattering spectra, leading to the dominant SOP mode [19]. Thus, the results in Fig. 3b confirm the fact of reducing the elastic deformations in the ZnO NS and reducing the concentration of point defects with thermal annealing.

The reaction kinetics of the MO dye degradation could be described by the pseudo-first-order model for low dye concentrations, i.e., $\ln(C/C_0) = K\ t$,

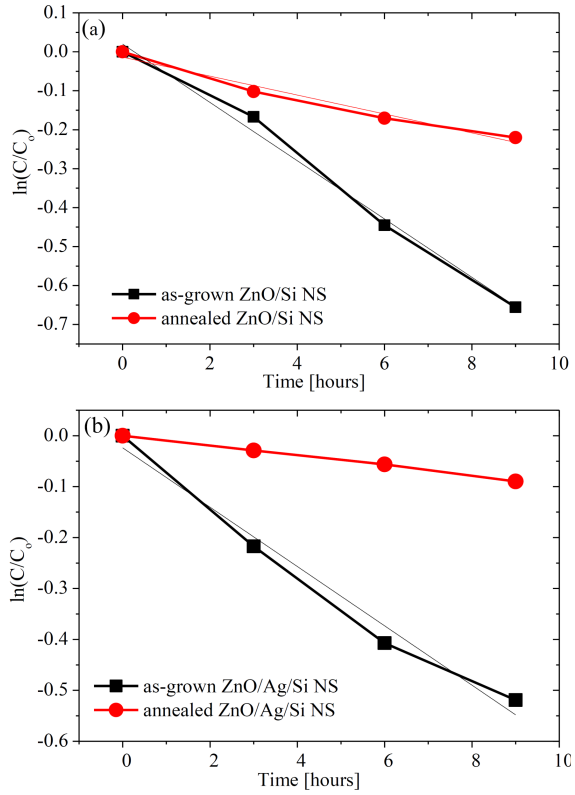

Fig. 4. Photodestruction of the MO dye for as-grown and annealed at 900°C ZnO/Si (a) and ZnO/Ag/Si (b) nanostructures under Hg lamp irradiation.

where C_0 and C are the concentrations of dye in the aqueous solution at time $t = 0$ and certain time t respectively, and K is the pseudo-first-order rate [20]. The photocatalysis of MO dye destruction with the help of ZnO/Si and ZnO/Ag/Si NS is shown in Fig. 4 in coordinates $\ln(C/C_0)$ vs time for K rate calculation. The photodestruction rate constant K was calculated to be 0.075 h^{-1} for as-grown ZnO/Si NS and 0.024 h^{-1} for annealed samples. For ZnO NS deposited on Ag/Si substrates, the photodestruction rate constant K was 0.058 h^{-1} for as-grown NS, and only 0.0098 h^{-1} for annealed ones.

The lower K value for ZnO/Ag/Si NS compared to ZnO/Si NS can be explained by a higher concentration of point defects generated in ZnO NS grown on the Ag/Si substrate. The lower intensity of NBE emission for ZnO/Ag/Si NS, in comparison to ZnO/Si NS, also indicates the lower concentration of free charges, which can apply in the photochemical process. The significant decrease in the rate of MO dye photodestruction with annealing can obviously be explained by a significant decrease in oxygen vacancies, as evidenced by the decrease in PL in the visible part of the spectrum. Oxygen vacancies provide conductivity in the films and nanostructures of zinc oxide, and obviously regulate the processes of charge transfer from the semiconductor to the dye. Thus, a necessary condition for improving photocatalytic properties is the presence of surface conductivity in the nanostructures and a good near band-edge photoluminescence.

4. Conclusions

In summary, the ZnO nanostructures were successfully grown on Si and Ag/Si substrates by atmospheric pressure metalorganic chemical vapor deposition method. The thin silver film was formed on Si substrates by the reaction of the silver mirror. The effect of thermal annealing on the structure and optical properties of ZnO nanostructures deposited on Si and Si substrates coated by silver film was investigated. It was shown that the photoluminescence in the visible part of the spectrum for ZnO/Si NS is much lower than for ZnO/Ag/Si NS, which is obviously due to different concentrations of oxygen vacancies and the influence of silver film surface morphology on the formation of zinc oxide nanostructures. Normalized PL spectra indicate almost the same integral intensity of UV PL for ZnO/Si NS both before and after annealing. Annealing of ZnO/Ag/Si NS significantly reduces PL in the visible part of the spectrum. PL spectra of ZnO/Ag/Si NS annealed at 900°C reveal the presence of an additional emission band at 475 nm, which may originate from optical transitions between shallow Zn_I donor levels and deep Ag_{Zn} acceptor levels testifying the incorporation of Ag ions into ZnO lattice in a small amount. Raman scattering study also confirms the reduction of point defects in ZnO/Si NS with annealing and indicates a significant improvement in the crystal lattice of ZnO/Ag/Si nanostructures. The significant decrease in the rate of photodestruction of the MO dye with annealing can obviously be explained by a significant decrease in oxygen vacancies.

Acknowledgments

This contribution was partially supported by the research project of NAS of Ukraine "Development of innovative photocatalytic nanostructured materials based on ZnO and TiO_2" and partially supported by the research project of NAS of Ukraine "The development of photocatalytic nanocomposites for viruses inactivation in the air".

References

[1] W. Xie, Y. Li, W. Sun, J. Huang, H. Xie, X. Zhao, *J. Photochem. Photobiol. A* **216**, 149 (2010).

[2] H. Bouzid, M. Faisal, F.A. Harraz, S.A. Al-Sayari, A.A. Ismail, *Catal. Today* **252**, 20 (2015).

[3] S. Kuriakose, V. Choudhary, B. Satpati, S. Mohapatra, *Beilstein J. Nanotechnol.* **5**, 639 (2014).

[4] A. Ievtushenko, V. Karpyna, J. Eriksson, I. Tsiaoussis, I. Shtepliuk, G. Lashkarev, R. Yakimova, V. Khranovskyy, *Superlattices Microstruct.* **117**, 121 (2018).

[5] Y. Zhang, B. Lin, X. Sun, Z. Fu, *Appl. Phys. Lett.* **86**, 131910 (2005).

[6] A. Galdámez-Martinez, G. Santana, F. Güell, P. R. Martínez-Alanis, A. Dutt, *Nanomaterials* **10**, 857 (2020).

[7] V. Karpyna, A. Ievtushenko, O. Kolomys, O. Lytvyn, V. Strelchuk, V. Tkach, S. Starik, V. Baturin, Î. Karpenko, *Phys. Status Solidi (b)* **257**, 1900788 (2020).

[8] Y. H. Ko, J. S. Yu, Phys. *Phys. Status Solidi (a)* **209**, 297 (2012).

[9] T. C. Damen, S. P. S. Porto, B. Tell, *Phys. Rev.* **142**, 570 (1966).

[10] S. K. Sharma, G. J. Exarhos, *Solid State Phenom.* **55**, 2 (1997).

[11] T. Gruber, G.M. Prinz, C. Kirchner, R. Kling, F. Reuss, W. Limmer, A. Waag, *J. Appl. Phys.* **96**, 289 (2004).

[12] W.-R. Liu, B.H. Lin, C.C. Kuo, W.C. Lee, M. Hong, J. Kwo, C.-H. Hsu, W.F. Hsieh, *Cryst. Eng. Comm.* **14**, 8103 (2012).

[13] R.J.V. Michael, B. Sambandam, T. Muthukumar, M.J. Umapathy, P.T. Manoharan, *Phys. Chem. Chem. Phys.* **16**, 8541 (2014).

[14] I. Martina, R. Wiesinger, D. Jembrih-Simbürger, M. Schreiner, *e-PS* **9**, 1 (2012).

[15] V.V. Strelchuk, O.F. Kolomys, B.O. Golichenko, M.I. Boyko, E.B. Kaganovich, I.M. Krishchenko, S.O. Kravchenko, O.S. Lytvyn, E.G. Manoilov, I.M. Nasieka, *Semicond. Phys. Quant. Electron. Optoelectron.* **18**, 46 (2015).

[16] M. Prasad, V. Sharma, R. Aher, A. Rokade, P. Ilaiyaraja, C. Sudakar, S. Jadkar, *J. Mater. Sci.* **52**, 13572 (2017).

[17] V.V. Strelchuk, A.S. Nikolenko, O.F. Kolomys, S.V. Rarata, K.A. Avramenko, P.M. Lytvyn, P.Tronc, C.O. Chey, O. Nur, M. Willander, *Thin Solid Films* **601**, 22 (2016).

[18] O.F. Kolomys, V.V. Strelchuk, S.V. Rarata, R. Hayn, A. Savoyant, F. Giovannelli, F. Delorme, V. Tkach, *Superlattice Microst.* **118**, 7 (2018).

[19] H. Zeng, W. Cai, B. Cao, J. Hu, Y. Li, P. Liu, *Appl. Phys. Lett.* **88**, 181905 (2006).

[20] M. Ahmad, E. Ahmed, Y. Zhang, N.R. Khalid, J. Xu, M. Ullah, Z. Hong, *Current Appl. Phys.* **13**, 697 (2013).